Construction and Building Materials 116 (2016) 422–430

Contents lists available at ScienceDirect

Construction and Building Materials

journal homepage: www.elsevier.com/locate/conbuildmat

Green lightweight cementitious composite incorporating aerogels and fly ash cenospheres – Mechanical and thermal insulating properties

Asad Hanif, Su Diao, Zeyu Lu, Tianyuan Fan, Zongjin Li *

Department of Civil and Environmental Engineering, The Hong Kong University of Science and Technology (HKUST), Clear Water Bay, Kowloon, Hong Kong Special Administrative Region

HIGHLIGHTS

- Ultra-lightweight cementitious composite was developed using aerogel and FAC.
- Both aerogel and FAC significantly reduce the density of resulting composites.
- Excellent thermal insulation properties and specific strength values are achieved.

ARTICLE INFO

Article history:
Received 28 November 2015
Received in revised form 10 April 2016
Accepted 26 April 2016
Available online 9 May 2016

Keywords:
Aerogel
Fly ash cenosphere
Lightweight
Cementitious composite
Thermal conductivity
Sustainable development

ABSTRACT

The research focused on the development of an ultra-lightweight cementitious composite with both excellent mechanical and thermal insulating properties. Fly ash cenosphere (FAC), and aerogel, a nano-structured highly porous material made of silica, were used as lightweight aggregates. Polyvinyl alcohol fibers were used to improve the mechanical behavior of the cementitious composite. The experimental results showed higher specific strength (up to 18 kPa/kg m^{-3}) of the resulting composites as compared to conventional lightweight materials. Depending on the amount of FAC and aerogel, the compressive and flexural strengths of the cementitious composite were found as 23.54–18.63 MPa and 4.94–3.66 MPa, respectively, while the thermal conductivity was reduced to 0.3197 W/m-K. Moreover, the hydration products and microstructures of the FAC/aerogel modified cementitious composite were investigated by the Scanning Electron Microscopy and Energy Dispersive X-ray Spectroscopy (EDS). Thermal stability of the hardened matrix was studied by using thermo-gravimetric analyses and it was revealed that the composites were fairly stable at a high temperature range. The weight loss varied with increasing aerogel content. In conclusion, both FAC and aerogel are excellent candidates for producing mechanically strong as well as thermally insulated composites which have great potential to be used in buildings for energy conservation.

1. Introduction

Lightweight concrete (LWC) is advantageous over normal weight concrete because of the reduction of dead loads, ease of handling, and better durability. LWC has been widely used in long-span bridges and floating marine structures [1,2]. Moreover, the better fire resistance [3] and thermal insulation properties [1] of the LWC further encourage its use in building structures such as roof coverings and facades, to improve the fire safety and thermal insulation properties of infrastructures. In the past decades, LWC has been developed using various kinds of lightweight aggregates (LWA) such as expanded perlite [4–9], hollow glass beads [8,10–13], expanded clay [8,14] and expanded polystyrene beads [13,15–19]. However, the conventionally used LWA requires various processing steps before utilizing in the cementitious composite, which not only increases their production cost but also releases the high amount of carbon dioxide emission associated with the processes which further raises concerns for the sustainable development. Furthermore, although the resulting composites have better thermal insulation properties, the poor mechanical properties hinder the use of such composites in load-bearing structures. Sengul et al. [5] experimentally investigated the effect of perlite aggregate on the mechanical and thermal properties of LWC and found that by replacing 60 vol.% of natural sand with expanded perlite, the strength reduction is about 84% which discourages its use in structural members. Nemes and Jozsa [12]

* Corresponding author.
E-mail address: zongjin@ust.hk (Z. Li).

http://dx.doi.org/10.1016/j.conbuildmat.2016.04.134
0950-0618/

also demonstrated that compressive strength of the cementitious composites incorporating expanded glass as lightweight fillers drastically decreased with the increasing volume fraction of the expanded glass, and the optimal amount of filler was found to be 48%. It was found by them that at 48% volume fraction of expanded glass aggregates, the strength was adequate (35 MPa) but the density was not low enough (1550 kg m^{-3}).

Recently, fly ash cenosphere (FAC) [2,20–25] and aerogel [26] have been studied for producing LWC. FAC is a byproduct of coal burning during electricity production process [27], which is lightweight (bulk density up to 800 kg m^{-3}) and cost effective. Wu et al. [28] conducted a series of experiments with various fractions of FAC and found that FAC is an excellent filler material for producing LWC which reduces the density of resulting concrete but the corresponding strength decrease is not substantial. They could produce lightweight composite having 28-day compressive strength of 49 MPa with density of 1240 kg m^{-3}. Also, Demirboga [29,30] showed that the thermal conductivity is affected due to the nature of the FAC which makes them a very reasonable choice for thermally insulated concrete as well. Moreover, aerogel is an extremely light (density 100 kg m^{-3}) nano-porous material composed of silica having a major volume (94–95%) being the air voids [31]. Gao et al. tried to produce LWC by using aerogel and found that using 60% of aerogel (by volume) the strength could reach only 8.3 MPa with the density being 1000 kg m^{-3}; which might be attributed to the low mechanical strength of the aerogel particles [32].

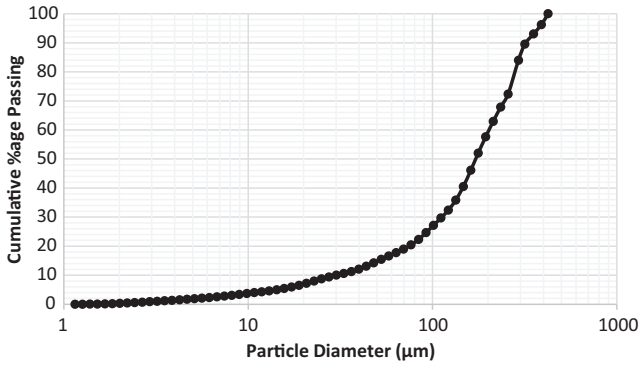

Fig. 1. Particle size analysis (by weight) of fly ash cenospheres.

Table 1
Physical properties of aerogels.

Density	Specific surface area	Particle size range	Porosity	Pore diameter	Hydrophobicity
40–150 kg m^{-3}	366.52 m^2/g	0.1–5 mm	>90%	20–100 nm	Super hydrophobic

Although the effects of FAC and aerogels on the cementitious composite were widely investigated, the co-effects of FAC/aerogels composites on the mechanical and thermal insulating properties of cementitious composite have not been conducted. The aim of current research is to develop an ultra-lightweight cement-based composite by incorporating FAC and aerogels that possesses not only excellent thermal insulation properties but also superior mechanical properties so that it can be efficiently used in building structures for energy conservation.

2. Experimental procedures

2.1. Materials

Ordinary Portland cement (OPC) type 52.5 was from Green Island, HK. Cement and silica fume were used to fabricate the binder. Fly Ash Cenospheres (FAC) were obtained from Zhen Yang Mineral Powder Processing Plant, Hebei China. The bulk density of the FAC particles was 720 kg m^{-3} and the particle sizes ranges from 60 to 360 μm, as shown in Fig. 1. The aerogel were obtained from Guangdong Alison Hi-Tech Co., Ltd (China). The physical properties of the aerogel are shown in Table 1. The specific surface area was measured by using Brunauer–Emmett–Teller (BET, Coulter SA 3100) analysis. The pore size distribution in aerogel is shown in Fig. 2. The PVA fiber (KURALON K-II REC15) used was 39 μm in diameter and 12 mm in length. The chemical composition of the raw materials analyzed by X-ray fluorescence spectrometer (XRF, JSX-3201Z) are listed in Table 2.

2.2. Mix design and specimen preparation

Table 3 enlists the six mix proportions of the cementitious composite with different FAC/aerogel composite contents. The water to binder ratio of all the mixes was set as 0.70 while the amount of FAC was 70% by weight of the binder. FAC and aerogel were used as the filler materials. A poly-carboxylate based admixture/super-plasticizer (ADVA 105 by Grace Inc. Canada) was used to maintain the homogeneity and consistency of the mixture.

The mixing procedure consisted of dry mixing of all the powders for one and a half minute followed by addition of 50% water while continuously mixing for another one and a half minute. Then the remaining water and super plasticizer were added and subjected to mixing of one minute. Finally the PVA fibers were gradually dispersed in the mix while continuously mixing which was continued for another four to five minutes until a homogeneous and consistent matrix was achieved. The mixing of fibers was done at a slow speed followed by high speed of the mixer thus maximizing the extent of uniformity of the mix.

The mixed slurry was cast into the molds and compacted for a small duration on a vibrating table to enable removal of entrapped air. Specimen of size 40 mm × 40 mm × 160 mm (for flexural strength testing), 40 mm × 40 mm × 40 mm (for compressive strength testing) and 350 mm × 350 mm × 20 mm (for evaluating thermal conductivity behavior) were cast for each mix. The specimens were kept sealed after casting at room temperature for 24 h and then de-molded.

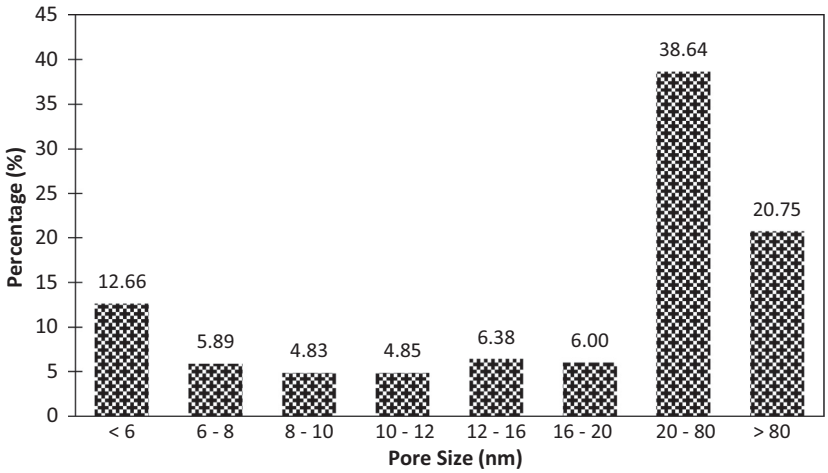

Fig. 2. Pore size distribution in aerogel particles.

Table 2
Chemical composition of raw materials.

Description	Cement	Silica fume	Fly ash cenospheres
Na_2O	–	–	2.42
Al_2O_3	3.86	–	16.7
SiO_2	19.47	98.45	73.1
SO_4	5.71	0.4	0.41
K_2O	0.49	0.31	3.94
CaO	65.4	0.77	1.05
TiO_2	0.26	–	0.35
MnO	–	–	0.05
Fe_2O_3	3.2	0.05	1.95
MgO	1.58	–	–

Table 3
Mix proportions (by weight).

Mix ID	Binder		Water	FAC	Aerogel	PVA fiber (wt.%)
	Cement	Silica fume				
FAC-A0	0.90	0.10	0.70	0.70	0%	1%
FAC-A1	0.90	0.10	0.70	0.70	1%	1%
FAC-A2	0.90	0.10	0.70	0.70	2%	1%
FAC-A3	0.90	0.10	0.70	0.70	3%	1%
FAC-A4	0.90	0.10	0.70	0.70	4%	1%
FAC-A5	0.90	0.10	0.70	0.70	5%	1%

Subsequently, the specimens were cured in a moist room under relative humidity of 95% at 25 °C until the testing age. The samples were tested for mechanical properties at the age of 10 days and 28 days.

2.3. Testing methods

2.3.1. Mechanical tests

The mechanical tests included flexural and compressive strength test. In order to evaluate the flexural performance of the composites, three-point bending test (Fig. 3(a)) was performed on the specimen with size 40 mm × 40 mm × 160 mm. A flexural testing setup, with force capacity of 250 kN, was used to apply load at the center point of prisms with a span length of 100 mm. Loading rate was set as 0.15 mm/min. Mid-span load and deflection were determined and subsequently corresponding stress and strain values as well as the elastic modulus were calculated using the following relations [33]:

$$\sigma_f = \frac{3PL}{2bd^2} \tag{1}$$

$$\varepsilon_f = \frac{6Dd}{L^2} \tag{2}$$

where, σ = stress in the outer fibers at midpoint, MPa, ε = strain in the outer surface, mm/mm, P = load at a given point on the load-deflection curve, N, L = support span, mm, b = width of beam tested, mm, d = depth of beam tested, mm, D = maximum deflection of the center of the beam, mm, and

Compressive strength testing (Fig. 3(b)) was done on the specimen, of size 40 mm × 40 mm × 40 mm, by crushing them in automatic compression testing machine (5000 kN capacity), subjected to the loading rate of 1.0 kN/s. The modulus of elasticity was calculated using ACI 318M-08 [34]. The relation used is shown in Eq. (4).

$$E_C = Wc^{1.5}(0.043)\sqrt{\lambda f'c} \tag{3}$$

where, Ec = modulus of elasticity of concrete, MPa, Wc = density (unit weight) of concrete, kg m^{-3}, f'c = compressive strength of concrete, MPa, and λ = modification factor reflecting the reduced mechanical properties of lightweight concrete.

The tested specimens were preserved for further morphological and microstructural characterization.

2.3.2. Thermal conductivity testing

Thermal conductivity of the specimen was determined using Quick Thermal Conductivity Meter (QTM-500 by Kyoto Electronics Manufacturing Co. Ltd, Japan) and averaged to estimate the representative value for each composite. The equipment can measure the thermal conductivity up to the range of 0.23–12 W/mK, and comprises of a probe sensor consisting of a single heating wire and thermocouple. The temperature of the wire increases in exponential progression when electric power is given to the probe. The heating wire is allowed to remain on the surface under testing for 60 s. Temperature rising curve is plotted versus time on logarithmic scale. The lower the thermal conductivity, the smaller the slope of the curve. The thermal conductivity is measured by the relation [35]:

$$\lambda = \frac{q \cdot \ln \frac{t2}{t1}}{4\pi(T2 - T1)} \tag{4}$$

where λ = Thermal conductivity of the sample (W/mK), q = Generated heat per unit length of sample/time (W/m), t_1, t_2 = measure time length (sec), T_1, T_2 = Temperature at t_1, t_2 (K).

The Experimental setup is shown in Fig. 4(a).

The behavior of the thermal insulating composites in real life situation (such as concrete panels used in facades or exterior walls or roof coverings for dissipating heat from the sun) was simulated in the laboratory with the help of an experimental setup consisting of an infra-red lamp of 275 W which acts as a heat source (mimicking sun) placed at a distance of 250 mm from the sample surface (of size 200 mm × 200 mm). Temperature sensors (thermocouples) were used to determine the temperature of the exterior surface (facing the lamp) as well as interior surface (the side opposite to the side facing the lamp). The thermocouples were connected to a computer which recorded the temperature at every second. Each specimen was subjected to a steady cycle of five hours of continuous heating. The heating cycles were plotted with temperature versus time and the difference of peak temperature between outer and inner surface was determined. The experimentation setup is demonstrated in Fig. 4(b).

Morphological and microstructural characterization was done by Scanning Electron Microscopy (SEM). SEM was carried out to characterize inner surface of the broken specimen as well as the hydration products. SEM examination was

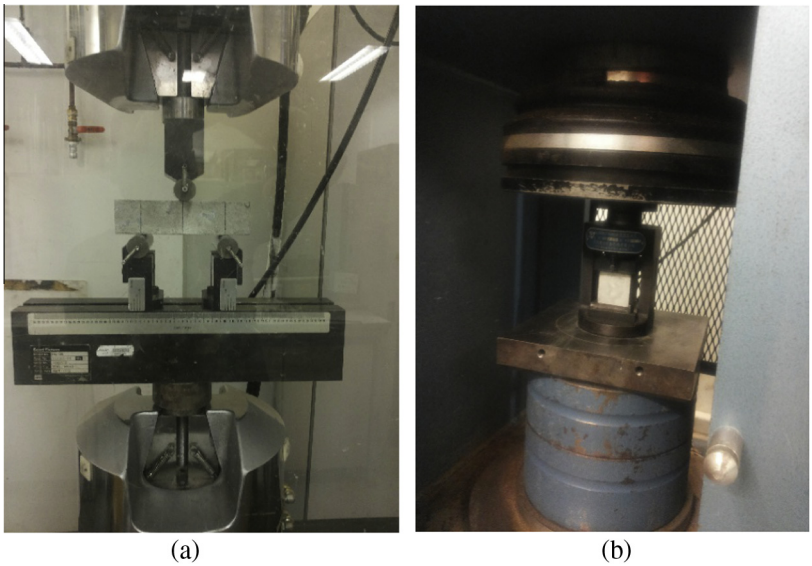

(a) (b)

Fig. 3. Three point flexural bending (a) and compressive strength (b) test setup.

(a) (b)

Fig. 4. Quick thermal conductivity measurement apparatus (a) and test setup for steady thermal conductivity behavior (b).

Table 4
Density of the specimens at different ages.

S. No	Mix ID	Unit weight (kg m^{-3})			
		Fresh mix	1-Day	28-Day SSD	28-Day OD
1	FAC-A0	1289	1201	1297	1098
2	FAC-A1	1221	1148	1250	1092
3	FAC-A2	1221	1153	1224	1050
4	FAC-A3	1173	1103	1201	1037
5	FAC-A4	1155	1081	1192	1014
6	FAC-A5	1144	1072	1187	1003

conducted by using JSM-6390 (JEOL) which was also equipped with the Energy Dispersive X-ray Spectroscopy (EDS) which enabled the mineralogical classification in the hydration products of the composites. The internal surface area and pore size distribution (pore volume characterization) of hardened pastes was determined by Brunauer–Emmett–Teller (BET) and Mercury Intrusion Porosimetry (MIP), respectively. Crushed specimens were broken down into smaller pieces and all the moisture in the specimen was removed by solvent replacement method. Methanol was used for this purpose and the specimens were immersed in methanol solution for one week during which the methanol was replaced every day with fresh supply of solution. After one week, the samples were vacuumed and dried.

3. Results and discussion

3.1. Density and mechanical properties

The density and mechanical properties are reported in Table 4 and Figs. 5, 6. The density was measured at the age of 1-day under normal condition and 28-days under either the saturated surface dry (SSD) condition or oven dry (OD) condition.

It is clearly seen that the 28-day SSD and OD density of all the composites are less than 1300 kg m^{-3} and the lightest one is only

Table 5
Compressive and flexural strength results at different ages.

S. No	Mix ID	Compressive strength (MPa)		Flexural behavior				
				10-Day		28-Day		
		10-Day	28-Day	Flexural strength (MPa)	Strain capacity (%)	Flexural strength (MPa)	Strain capacity (%)	Elastic modulus (GPa) [34]
1	FAC-A0	21.98	23.54	3.89	0.260	4.94	0.624	8.44
2	FAC-A1	18.78	22.89	3.47	0.301	4.52	0.773	7.88
3	FAC-A2	18.56	21.58	3.40	0.351	4.25	0.475	7.41
4	FAC-A3	17.31	20.25	3.18	0.731	4.21	0.715	6.98
5	FAC-A4	16.88	19.86	2.98	0.740	3.90	0.541	6.83
6	FAC-A5	15.58	18.63	2.84	0.632	3.66	0.698	6.57

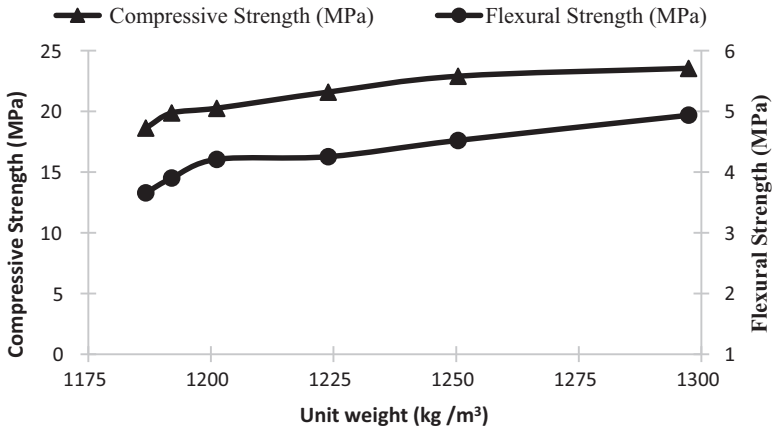

Fig. 5. Plot of strength versus SSD unit weight (28-day).

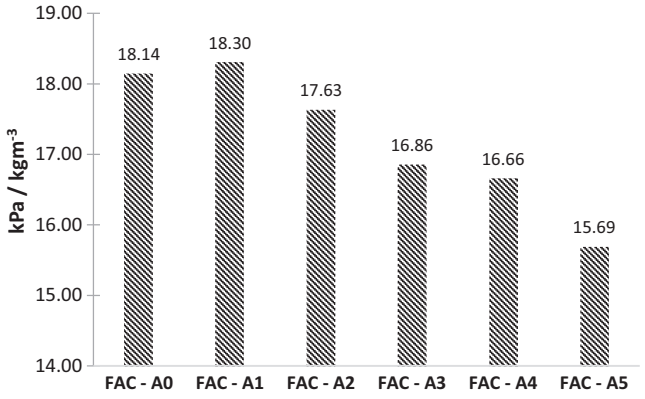

Fig. 6. Specific strength values at 28-day age.

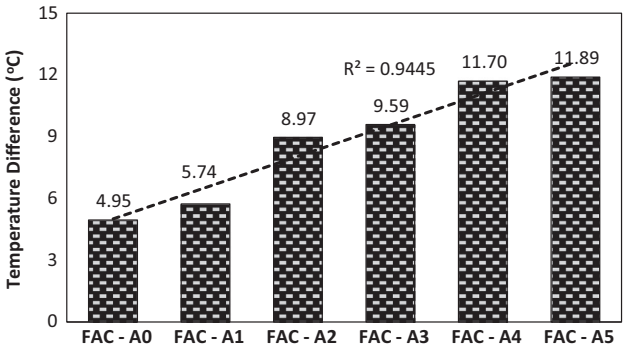

Fig. 8. Peak temperature difference between inner and outer surface during steady thermal test.

1003 kg m^{-3}, which clearly indicates its classification as ultra-lightweight concrete [36]. However, aerogel has limited effects on reducing the density of the composite, which might result from the air voids-filling effect.

The compressive and flexural strength of the composites with different density were measured at 10-day and 28-day age and the results are shown in Table 5 and Fig. 5. It is obvious that the compressive and flexural strengths decrease with the decrease of the density of the mixture. The specific strength (ratio of compressive strength and density) at 28-day age is plotted as Fig. 6. It can be seen that the composites even with lower compressive strength values resulted in higher values of specific strength due to the ultra-lightweight nature. The lowest specific strength found was 15.7 which means that this particular composite (FAC-A5) is equivalent in strength to a normal weight concrete (of density 2400 kg m^{-3}) having compressive strength of 38 MPa approximately which indicates adequate level of mechanical properties.

3.2. Thermal conductivity

The values of thermal conductivity coefficient at ambient temperature (25 °C) are shown in Fig. 7. It can be clearly seen that the FAC and aerogel particles reduce the thermal conductivity of the composite. As the weight fraction of FAC was kept constant in all the mixes, the only parameter further reducing the thermal conductivity is aerogel. Up to 23.3% reduction in thermal conductivity is observed when 5% weight fraction of aerogel is incorporated in the mixtures. The reasons for such lower thermal conductivity are the hollow structure of the FAC, the air voids entrapped within the composite, and the open nano-porous nature of aerogel particles. The findings are in consistence with the existing studies on thermal conductivity of concretes containing high volumes of fly ash [37,38] (as the production of FAC and fly ash involves the same process and raw material, and the only difference is the particle size, so it is reasonable to make such comparison).

The specimens were also subjected to steady thermal test and the results are summarized in Figs. 8 and 9. The steady thermal tests show the results consistent with the findings from quick thermal conductivity measurement and it can be seen that the difference of peak temperature between exterior and interior surface (Fig. 9) increases with the increase of aerogel content. It is obvious that 5 wt.% aerogel leads to 12 °C temperature difference, which is 7 °C higher than that of specimen without aerogel. The decreased thermal conductivity and increased temperature difference is attributed to the increased pore volume of the composite with increasing contents of aerogel. The increased pore volume with increasing aerogel amount was verified by BET and MIP analyses. The measured BET surface area values and corresponding pore volume are plotted in Fig. 10. These results corroborated the increased pore volume. It can be seen that increase in aerogel amount leads to the increase of the total pore volume which was expected because of the open nano-porous structure of aerogel particles.

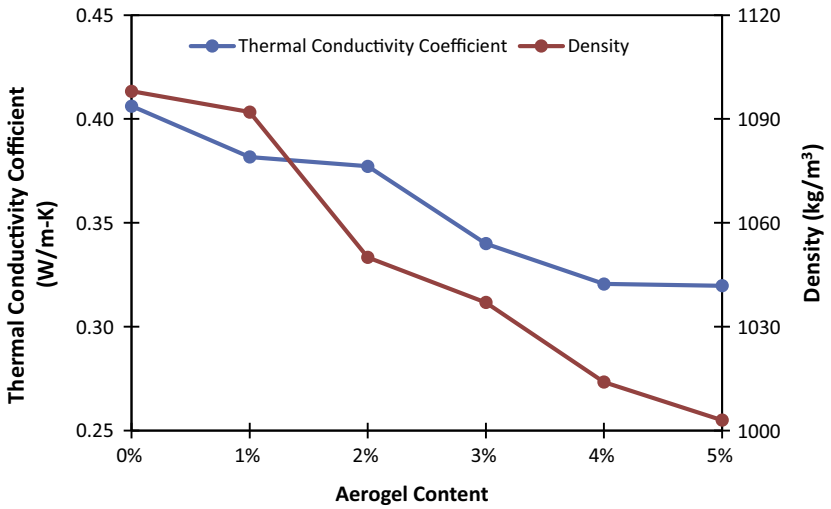

Fig. 7. Thermal conductivity coefficient values.

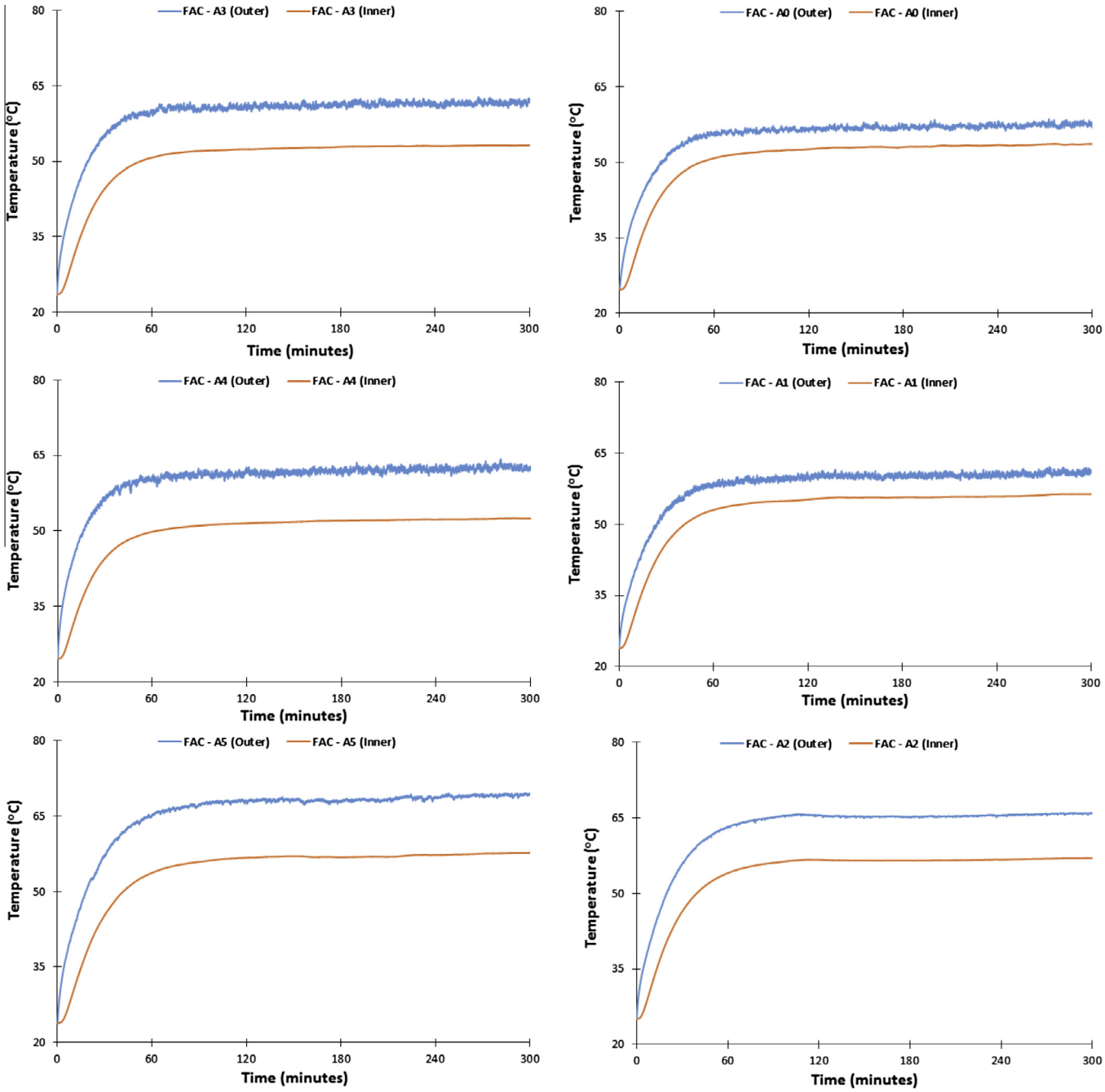

Fig. 9. Steady thermal test results.

With every 1 wt.% increase of aerogel content, the pore volume increased by about 1.6%.

3.3. Morphological and microstructural characterization

The scanning electron microscopic (SEM) images are shown in Fig. 11, which indicate the inert nature of silica aerogels. The aerogel particles remained unreacted in the composites while partially broken FAC shells show moderate reactivity of FAC particles. Energy dispersive X-ray spectroscopy (EDS) was done to further identify and observe the aerogel particles (Figs. 12 and 13) within the cement matrix but due to the translucent nature of aerogel particles, the incident beam of electrons focused on the particular particle may not excite it rather the result obtained thereof represent reaction products underneath. Figs. 12 and 13 show the usual hydration products along with FAC and aerogel particles. Also, from the Fig. 13, it can be seen that silica is dispersed all over the area (under examination of EDS) indicating dispersed aerogel particles.

Mercury intrusion porosimetry (MIP) results are summarized and plotted in Figs. 14 and 15. The porosity values range from 43.94% to 50.69% with FAC-A0 (reference mix) being the lowest. The porosity is found to be increasing with increase of aerogel content in the composites. The results show a direct co-relation of porosity with aerogel content which is due to the open porous nature of the aerogel particles. At higher levels of aerogel addition i.e.

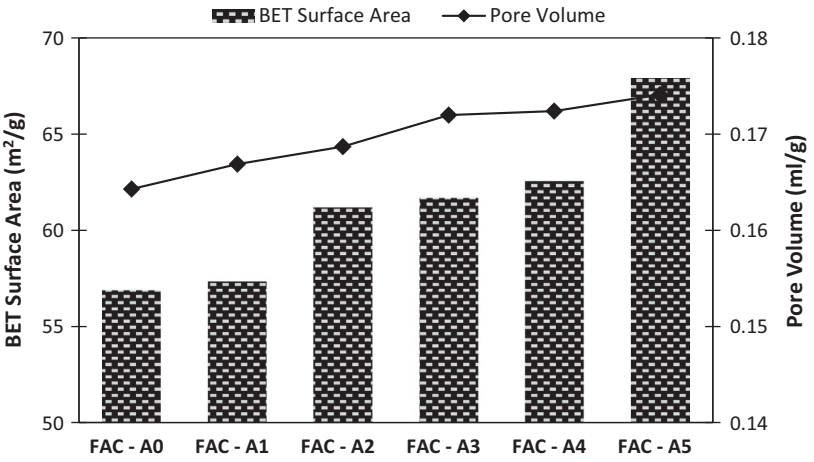

Fig. 10. Measured BET surface area and pore volume of the composites.

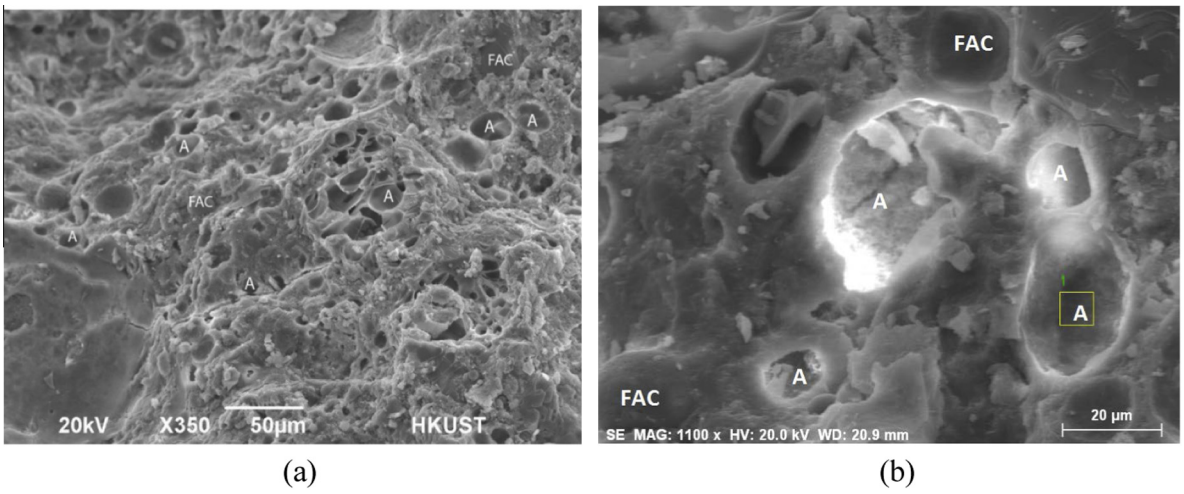

Fig. 11. SEM images of hardened composite showing the presence of fly ash cenosphere (FAC) and aerogel (A).

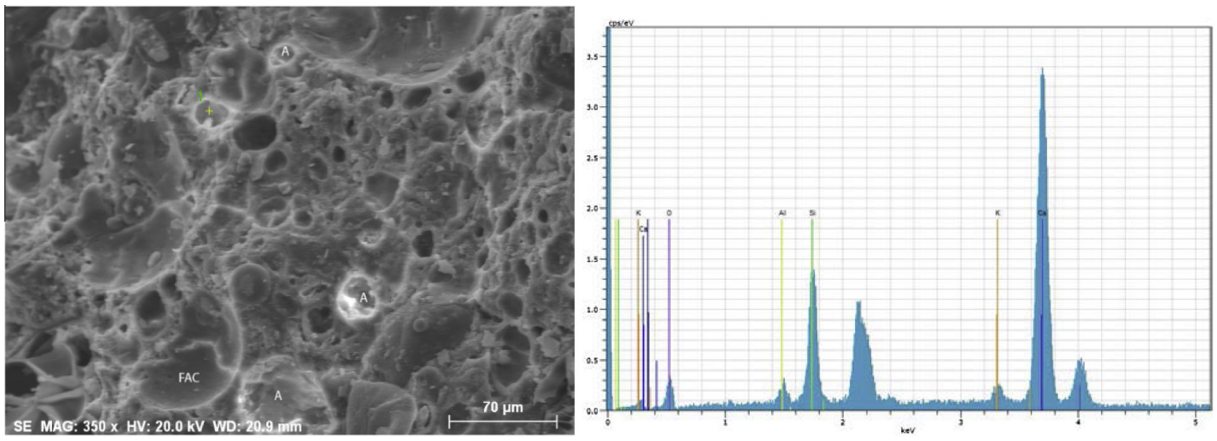

Fig. 12. SEM/EDS analysis of specimen.

4% and 5%, although there is increase in porosity but the increment is not very high which may be attributed to the agglomeration of the particles. The pore size distributions are plotted and shown in Fig. 15 which depicts the presence of greater fraction of micro-pores (size less than 2 nm) and meso-pores (size from 2 to 50 nm) in composites containing aerogel (FAC-A1 through FAC-A5) as compared to the reference mix (FAC-A0). Although, the porosity directly increases with increase of aerogel weight fraction,

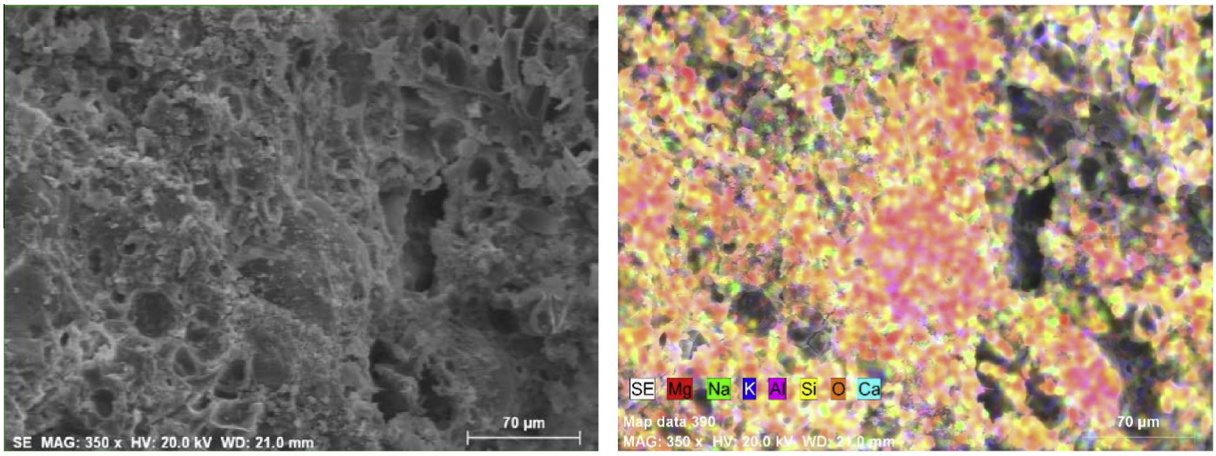

Fig. 13. EDS spectrum of an area of FAC-aerogel modified composite.

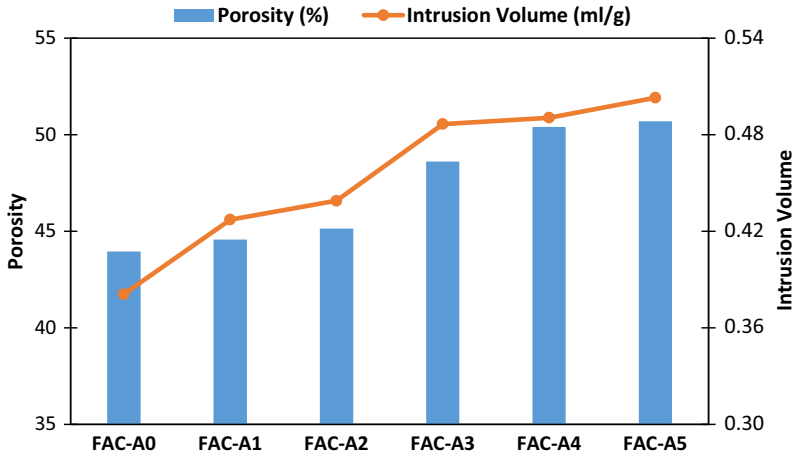

Fig. 14. Mercury intrusion porosimetry (MIP) results.

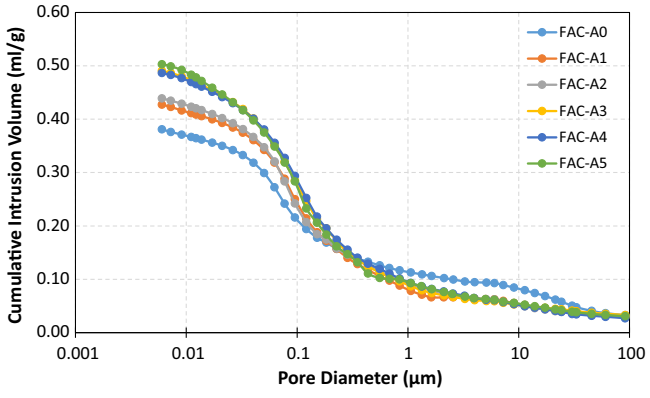

Fig. 15. Cumulative intrusion volume curves (from MIP).

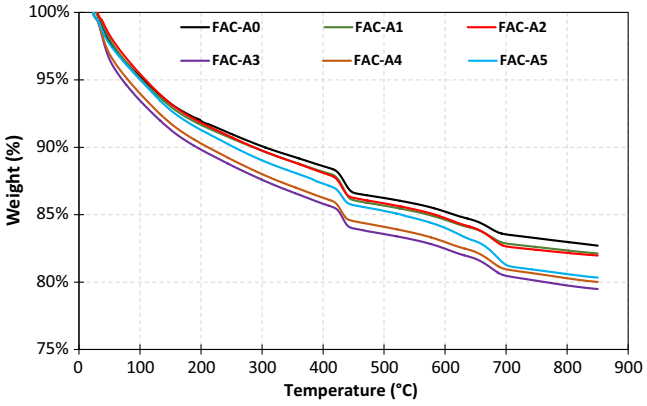

Fig. 16. TGA weight loss curves.

however it has been found that these pores are not generally interconnected. This may be due to the agglomeration of the aerogel particles creating barriers among the pores.

Thermogravimetric analyses (TGA) results are shown in Fig. 15. It can be seen that varying the aerogel content in the composites affects both the de-hydroxylation and de-carbonation peaks. Increasing the aerogel content further lowers the weight loss curve. However, it has been observed that the weight loss curves do not show a general trend/pattern with increasing aerogel content which might be due to non-homogeneity of the composites. Although, the total weight loss %age for aerogel modified cementitious composite is lower than the reference composite (FAC-A0), still it can be seen from the Fig. 16 that the composites are fairly stable at higher temperature range.

4. Conclusions

In this study, ultra-lightweight cement-based composites were successfully developed by using FAC and aerogel as aggregate. The composites were found complying with the ACI specifications of structural lightweight concrete (density in the range of 1120–1920 kg m^{-3} and minimum compressive strength of 17 MPa at 28 days). The resulting composites have better mechanical properties due to the presence of FAC which also possess some degree of reactivity while thermal insulating behavior is also improved due to hollow structure of FAC particles and open-porous nature of aerogel particles. Utilization of aerogel in the composite also helped reducing the permeability which shows better durability related properties for such composites. In addition, the excellent thermal insulation properties of aerogel incorporated composites make them desirable for use in buildings and construction for energy conservation while the adequate mechanical strength (compressive strength ranging from 23.54 to 18.63 and flexural strength ranging from 4.94 to 3.63) make them suitable for the applications as structural members.

References

[1] ACI 213, Guide for Structural Lightweight-Aggregate Concrete, 2003.
[2] X. Huang, R. Ranade, Q. Zhang, W. Ni, V.C. Li, Mechanical and thermal properties of green lightweight engineered cementitious composites, Constr. Build. Mater. 48 (2013) 954–960, http://dx.doi.org/10.1016/j.conbuildmat.2013.07.104.
[3] ACI 216.1, Standard Method for Determining Fire Resistance of Concrete and Masonry Construction Assemblies, 1997.
[4] D. Kramar, V. Bindiganavile, Impact response of lightweight mortars containing expanded perlite, Cem. Concr. Compos. 37 (2013) 205–214, http://dx.doi.org/10.1016/j.cemconcomp.2012.10.004.
[5] O. Sengul, S. Azizi, F. Karaosmanoglu, M.A. Tasdemir, Effect of expanded perlite on the mechanical properties and thermal conductivity of lightweight concrete, Energy Build. 43 (2011) 671–676, http://dx.doi.org/10.1016/j.enbuild.2010.11.008.
[6] D. Kramar, V. Bindiganavile, Mechanical properties and size effects in lightweight mortars containing expanded perlite aggregate, Mater. Struct. 44 (2010) 735–748, http://dx.doi.org/10.1617/s11527-010-9662-0.
[7] İ.B. Topçu, B. Işıkdağ, Effect of expanded perlite aggregate on the properties of lightweight concrete, J. Mater. Process. Technol. 204 (2008) 34–38, http://dx.doi.org/10.1016/j.jmatprotec.2007.10.052.
[8] V. Ducman, A. Mladenovic, Alkali–silica reactivity of some frequently used lightweight aggregates, Cem. Concr. Res. 34 (2004) 1809–1816, http://dx.doi.org/10.1016/j.cemconres.2004.01.017.
[9] Z. Lu, B. Xu, J. Zhang, Y. Zhu, G. Sun, Z. Li, Preparation and characterization of expanded perlite/paraffin composite as form-stable phase change material, Sol. Energy 108 (2014) 460–466, http://dx.doi.org/10.1016/j.solener.2014.08.008.
[10] C. Shi, K. Zheng, A review on the use of waste glasses in the production of cement and concrete, Resour. Conserv. Recycl. 52 (2007) 234–247, http://dx.doi.org/10.1016/j.resconrec.2007.01.013.
[11] C. Shi, Y. Wu, Mixture Proportioning and Properties of Self-Consolidating Lightweight Concrete Containing Glass Powder, 2005.
[12] R. Nemes, Z. Józsa, Strength of Lightweight Glass Aggregate Concrete, J. Mater. Civ. Eng. (2006) 710–714.
[13] M.L. Torres, P.A. García-Ruiz, Lightweight pozzolanic materials used in mortars: evaluation of their influence on density, mechanical strength and water absorption, Cem. Concr. Compos. 31 (2009) 114–119, http://dx.doi.org/10.1016/j.cemconcomp.2008.11.003.
[14] S. Ghourchian, M. Wyrzykowski, P. Lura, M. Shekarchi, B. Ahmadi, An investigation on the use of zeolite aggregates for internal curing of concrete, Constr. Build. Mater. 40 (2013) 135–144, http://dx.doi.org/10.1016/j.conbuildmat.2012.10.009.
[15] K. Miled, K. Sab, R. Le Roy, Particle size effect on EPS lightweight concrete compressive strength: experimental investigation and modelling, Mech. Mater. 39 (2007) 222–240, http://dx.doi.org/10.1016/j.mechmat.2006.05.008.
[16] D. Bouvard, J.M. Chaix, R. Dendievel, A. Fazekas, J.M. Létang, G. Peix, et al., Characterization and simulation of microstructure and properties of EPS lightweight concrete, Cem. Concr. Res. 37 (2007) 1666–1673, http://dx.doi.org/10.1016/j.cemconres.2007.08.028.
[17] R. Le Roy, E. Parant, C. Boulay, Taking into account the inclusions' size in lightweight concrete compressive strength prediction, Cem. Concr. Res. 35 (2005) 770–775, http://dx.doi.org/10.1016/j.cemconres.2004.06.002.
[18] R. Baetens, B.P. Jelle, J.V. Thue, M.J. Tenpierik, S. Grynning, S. Uvsløkk, et al., Vacuum insulation panels for building applications: a review and beyond, Energy Build. 42 (2010) 147–172, http://dx.doi.org/10.1016/j.enbuild.2009.09.005.
[19] B. Chen, N. Liu, A novel lightweight concrete-fabrication and its thermal and mechanical properties, Constr. Build. Mater. 44 (2013) 691–698, http://dx.doi.org/10.1016/j.conbuildmat.2013.03.091.
[20] J.-Y. Wang, K.-S. Chia, J.-Y.R. Liew, M.-H. Zhang, Flexural performance of fiber-reinforced ultra lightweight cement composites with low fiber content, Cem. Concr. Compos. 43 (2013) 39–47, http://dx.doi.org/10.1016/j.cemconcomp.2013.06.006.
[21] M.R. Wang, D.C. Jia, P.G. He, Y. Zhou, Microstructural and mechanical characterization of fly ash cenosphere/metakaolin-based geopolymeric composites, Ceram. Int. 37 (2011) 1661–1666, http://dx.doi.org/10.1016/j.ceramint.2011.02.010.
[22] X. Liu, K.S. Chia, M.-H. Zhang, Development of lightweight concrete with high resistance to water and chloride-ion penetration, Cem. Concr. Compos. 32 (2010) 757–766, http://dx.doi.org/10.1016/j.cemconcomp.2010.08.005.
[23] L.N. Ngu, H. Wu, D.K. Zhang, Characterization of ash cenospheres in fly ash from Australian power stations, Energy Fuels 21 (2007) 3437–3445, http://dx.doi.org/10.1021/ef700340k.
[24] J.Y. Wang, M.H. Zhang, W. Li, K.S. Chia, R.J.Y. Liew, Stability of cenospheres in lightweight cement composites in terms of alkali-silica reaction, Cem. Concr. Res. 42 (2012) 721–727, http://dx.doi.org/10.1016/j.cemconres.2012.02.010.
[25] J.Y. Wang, Y. Yang, J.Y.R. Liew, M.H. Zhang, Method to determine mixture proportions of workable ultra lightweight cement composites to achieve target unit weights, Cem. Concr. Compos. 53 (2014) 178–186, http://dx.doi.org/10.1016/j.cemconcomp.2014.07.006.
[26] T. Gao, B.P. Jelle, A. Gustavsen, S. Jacobsen, Aerogel-incorporated concrete: an experimental study, Constr. Build. Mater. 52 (2014) 130–136, http://dx.doi.org/10.1016/j.conbuildmat.2013.10.100.
[27] E.V. Fomenko, N.N. Anshits, M.V. Pankova, L.A. Solovyov, A.G. Anshits, Fly Ash Cenospheres: Composition, Morphology, Structure, and Helium Permeability, in: World Coal Ash Conf. – May 9–12, Denver, CO, USA, 2011.
[28] Y. Wu, J.-Y. Wang, P.J.M. Monteiro, M.-H. Zhang, Development of ultra-lightweight cement composites with low thermal conductivity and high specific strength for energy efficient buildings, Constr. Build. Mater. 87 (2015) 100–112, http://dx.doi.org/10.1016/j.conbuildmat.2015.04.004.
[29] R. Demirboğa, Thermal conductivity and compressive strength of concrete incorporation with mineral admixtures, Build. Environ. 42 (2007) 2467–2471, http://dx.doi.org/10.1016/j.buildenv.2006.06.010.
[30] R. Demirboğa, Influence of mineral admixtures on thermal conductivity and compressive strength of mortar, Energy Build. 35 (2003) 189–192, http://dx.doi.org/10.1016/S0378-7788(02)00052-X.
[31] A.C. Pierre, G.M. Pajonk, Chemistry of aerogels and their applications, Chem. Rev. 102 (2002) 4243–4265.
[32] T. Woignier, J. Phalippou, Mechanical strength of silica aerogels, J. Non Cryst. Solids 100 (1988) 404–408, http://dx.doi.org/10.1016/0022-3093(88)90054-3.
[33] ASTM D790-10, Standard Test Methods for Flexural Properties of Unreinforced and Reinforced Plastics and Electrical Insulating Materials, 2010, http://dx.doi.org/10.1520/D0790-10.
[34] ACI Committee 318, Building Code Requirements for Structural Concrete (ACI 318M-08), 2007.
[35] S.W. Tang, E. Chen, H.Y. Shao, Z.J. Li, A fractal approach to determine thermal conductivity in cement pastes, Constr. Build. Mater. 74 (2015) 73–82, http://dx.doi.org/10.1016/j.conbuildmat.2014.10.016.
[36] Z. Li, Advanced Concrete Technology, John Wiley & Sons Inc, 2011.
[37] D. Bentz, M. Peltz, A. Duran-Herrera, P. Valdez, C. Juarez, Thermal properties of high-volume fly ash mortars and concretes, J. Build. Phys. 34 (2011) 263–275, http://dx.doi.org/10.1177/1744259110376613.
[38] A. Arizmendi-Morquecho, A. Chávez-Valdez, J. Alvarez-Quintana, High temperature thermal barrier coatings from recycled fly ash cenospheres, Appl. Therm. Eng. 48 (2012) 117–121, http://dx.doi.org/10.1016/j.applthermaleng.2012.05.004.